ACS NANO
Cite This: ACS Nano 2018, 12, 4868−4876
www.acsnano.org

ARTICLE

Strong Capillarity, Chemisorption, and Electrocatalytic Capability of Crisscrossed Nanostraws Enabled Flexible, High-Rate, and Long-Cycling Lithium−Sulfur Batteries

Lianbo Ma,[†] Wenjun Zhang,[†] Lei Wang,[†] Yi Hu,[†] Guoyin Zhu,[†] Yanrong Wang,[†] Renpeng Chen,[†] Tao Chen,[†] Zuoxiu Tie,[†] Jie Liu,[†,‡] and Zhong Jin*[,†]

[†]Key Laboratory of Mesoscopic Chemistry of MOE, School of Chemistry and Chemical Engineering, Nanjing University, Nanjing, Jiangsu 210023, China

[‡]Department of Chemistry, Duke University, Durham, North Carolina 27708, United States

Supporting Information

ABSTRACT: The development of flexible lithium−sulfur (Li−S) batteries with high energy density and long cycling life are very appealing for the emerging flexible, portable, and wearable electronics. However, the progress on flexible Li−S batteries was limited by the poor flexibility and serious performance decay of existing sulfur composite cathodes. Herein, we report a freestanding and highly flexible sulfur host that can simultaneously meet the flexibility, stability, and capacity requirements of flexible Li−S batteries. The host consists of a crisscrossed network of carbon nanotubes reinforced CoS nanostraws (CNTs/CoS-NSs). The CNTs/CoS-NSs with large inner space and high conductivity enable high loading and efficient utilization of sulfur. The strong capillarity effect and chemisorption of CNTs/CoS-NSs to sulfur species were verified, which can efficiently suppress the shuttle effect and promote the redox kinetics of polysulfides. The sulfur-encapsulated CNTs/CoS-NSs (S@CNTs/CoS-NSs) cathode in Li−S batteries exhibits superior performance, including high discharge capacity, rate capability (1045 mAh g^{-1} at 0.5 C and 573 mAh g^{-1} at 5.0 C), and cycling stability. Intriguingly, the soft-packed Li−S batteries based on S@CNTs/CoS-NSs cathode show good flexibility and stability upon bending.

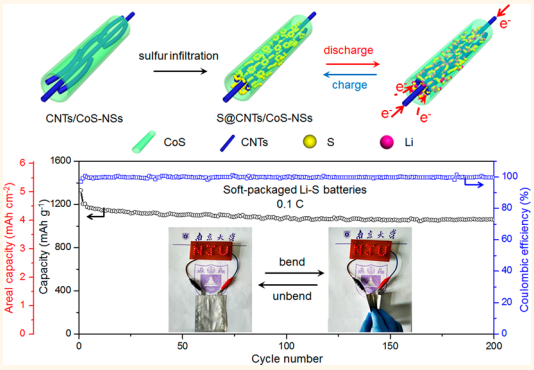

KEYWORDS: *lithium−sulfur batteries, flexible sulfur host, CoS nanostraws, capillarity effect and chemisorption, soft-packed pouch cells*

The recent prosperity in flexible and wearable electronics calls for energy storage systems with great flexibility, high energy density, and long cycling life.[1−7] Among the current options, lithium−sulfur (Li−S) batteries have become one of the most promising next-generation power sources because of many conspicuous advantages including high theoretical specific capacity endowed by multielectron conversion reaction, abundant natural reserves, low cost, and environmental benign,[8−12] which can fulfill the urgent demands of thriving consumer electronics market. Especially, flexible Li−S batteries are a very attractive candidate to realize exceptional portability and applicability for different scenarios, such as rolled-up displays, implantable devices, touch screens, conformable active radio frequency identification tags, epidermal sensors, and artificial skins.[13−18] However, the application of flexible Li−S batteries may suffer from the poor mechanical properties of sulfur cathodes, decreased electrical conductivity under deformation, unsatisfactory interfacial structure for electrolyte infiltration and polysulfide preservation, and so on.[19] By now, although numerous nanostructured sulfur hosts have been developed to alleviate these issues,[20−25] very few solutions can simultaneously meet all the flexibility, capacity, and stability requirements of flexible Li−S batteries.

In this work, we report the design of a crisscrossed network of carbon nanotubes (CNTs) reinforced hollow CoS nanostraws (CNTs/CoS-NSs) as a flexible sulfur host matrix. With the intriguing hollow structures, high conductivity, strong

Received: March 7, 2018
Accepted: April 23, 2018
Published: April 23, 2018

DOI: 10.1021/acsnano.8b01763
ACS Nano 2018, 12, 4868−4876

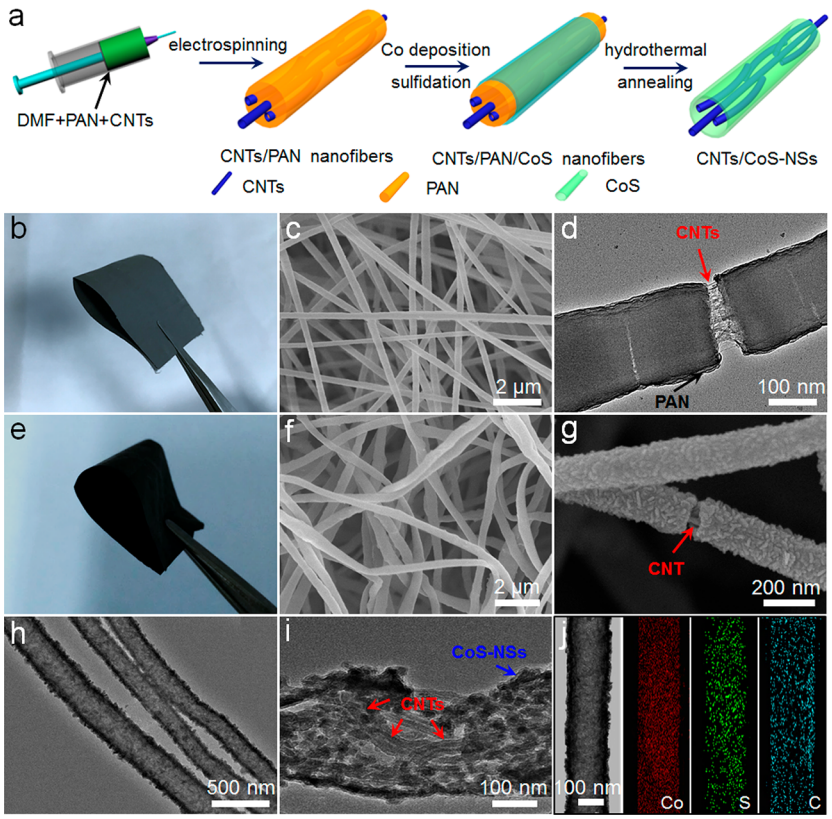

Figure 1. (a) Schematic of the synthesis process of CNTs/CoS-NSs. (b) Photograph, (c) SEM, and (d) TEM images of the freestanding and flexible crisscrossed network of precursor CNTs/PAN nanofibers. (e) Photograph, (f, g) SEM and (h, i) TEM images of as-obtained CNTs/CoS-NSs. (j) TEM image and corresponding elemental mappings of S@CNTs/CoS-NSs.

capillarity effect and chemisorption to sulfur species, and eletrocatalytic effect for rapid polysulfide conversion, the sulfur-filled CNTs/CoS-NSs (S@CNTs/CoS-NSs) cathode exhibits excellent electrochemical performances. Moreover, the intensive capillarity of lyophilic nanostraws can well retain the electrolyte, which can provide sufficiently wetted and infiltrated interface between electrolyte and active sulfur, thus conducive to achieve superb sulfur utilization and areal capacity. As a result, the soft-packaged Li−S pouch cells based on S@CNTs/CoS-NSs cathodes exhibited good cycling stability even under bending-unbending operations.

RESULTS AND DISCUSSION

The synthesis process of CNTs/CoS-NSs is schematically illustrated in Figure 1a and detailed in the Experimental Section. First, CNTs/PAN nanofibers with CNTs embedded in polyacrylonitrile (PAN) were prepared through an electrospinning method. Then, a CoS layer was formed through the coating of Co-containing species onto CNTs/PAN fibers and followed by a sulfidation step. After that, a solution-phase treatment converted the PAN nanofibers into hydrosoluble poly(acrylic acid) (PAA) through the hydrolysis of C≡N groups to COOH and NH_3. The hydrosoluble PAA was completely dissolved and removed in water to create hollow nanostraws, achieving the synthesis of CNTs/CoS-NSs. It should be noted that a thin layer of carbon shell derived from the carbonization of glucose may be coated on the surface of CNTs/CoS-NSs during the hydrothermal process, which can further enhance the electrical conductivity of CNTs/CoS-NSs and improve the structural flexibility and integrity of sulfur cathodes during cycling.

Figure 1b presents the optical image of precursor CNTs/PAN nanofibers, showing the freestanding and highly flexible traits. The scanning electron microscopy (SEM) image of CNTs/PAN nanofibers in Figure 1c reveals that the crisscrossed network structure consists of uniform nanofibers with several centimeters in length and ∼200 nm in diameter. The CNTs/PAN nanofibers exhibit smooth surface characteristics, with no CNTs protruding out of the surface. Further transmission electron microscopy (TEM) characterization of a crack in a CNTs/PAN nanofiber reveals the presence of embedded CNTs, as marked in Figure 1d. The as-prepared CNTs/CoS-NSs can almost preserve the flexibility and morphology of precursor CNTs/PAN nanofibers (Figure 1e). The SEM image (Figure 1f) demonstrates that CNTs/CoS-NSs retain the morphology of initial CNTs/PAN nanofibers but with the average diameter increased to ∼240 nm. The CNTs/CoS-NSs exhibit a rougher surface characteristic as compared with CNTs/PAN nanofibers, owing to the formation of CoS layer. Moreover, the CNTs embedded in CNTs/CoS-NSs can be observed from the fissure, as indicated in Figure 1g. The TEM images (Figure 1h, i) disclose the interior hollow structure of CNTs/CoS-NSs originated from the completely removal of PAN. The deep contrast of CoS layer makes the CNTs almost indistinguishable under TEM observation (Figure 1h). Nevertheless, TEM image of broken nanotube with higher magnification (Figure 1i) still shows that the CNTs are wrapped inside the CoS nanostraws. The CNTs can guarantee the high flexibility and smooth electron transfer of CNTs/CoS-NSs. Further high-resolution TEM (HRTEM) characterization in Figure S1 discloses a lattice distance of 0.29 nm, which can be indexed to the (100) planes of CoS.

DOI: 10.1021/acsnano.8b01763
ACS Nano 2018, 12, 4868−4876

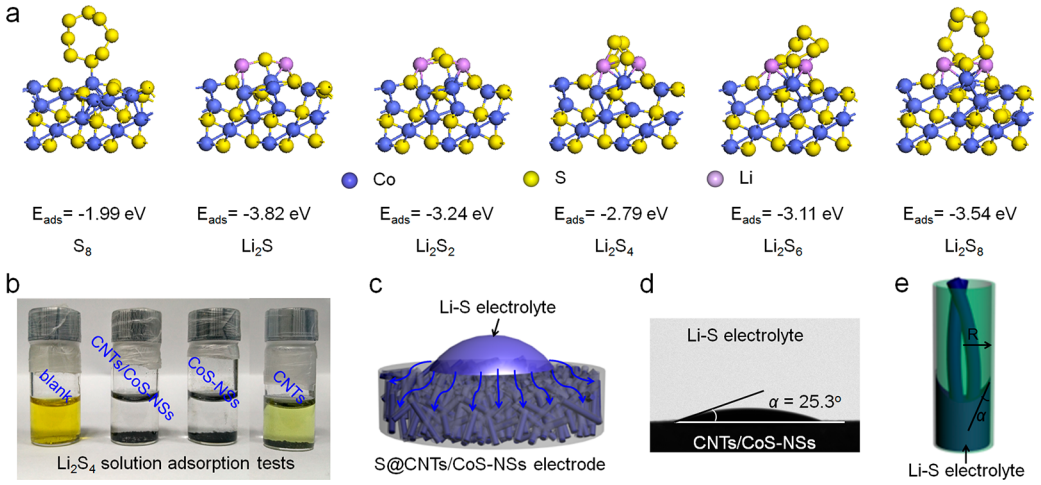

Figure 2. (a) Theoretical structure configurations and binding energies between the (101) planes of CoS and various sulfur species (S_8 and S_x^{2-}, $1 \le x \le 8$), indicating the strong chemisorption between CoS and sulfur species. (b) Adsorption capability tests of CNTs/CoS-NSs, CoS-NSs, and CNTs in mixed DOL/DME solutions of 0.02 M Li_2S_4. (c) Schematic of the wetting and infiltration of Li−S electrolyte within S@CNTs/CoS-NSs electrode. (d) Contact angle measurement of Li−S electrolyte on CNTs/CoS-NSs surface. (e) The capillary phenomenon diagram of Li−S electrolyte absorbed inside CNTs/CoS-NSs.

After the sulfur encapsulation, the compositions of S@CNTs/CoS-NSs were investigated by elemental mappings (Figure 1j), showing the co-existence of Co, S, and C elements and demonstrating their homogeneous distribution in the tubular structure.

Figure S2 shows the X-ray diffraction (XRD) pattern of CNTs/CoS-NSs, presenting the typical diffraction peaks of CoS (JCPDS card, no. 65-3418). After the filling of sulfur, additional XRD peaks belonging to elemental sulfur are observed, suggesting the formation of S@CNTs/CoS-NSs. X-ray photoelectron spectroscopy (XPS) was performed to investigate the compositions and chemical states of S@CNTs/CoS-NSs (Figure S3a); the detected elements were Co, S, and C, consistent with the result of elemental mappings. High-resolution XPS spectrum at Co 2p region (Figure S3b) revealed two distinguished doublets of Co $2p_{3/2}$ and Co $2p_{1/2}$ energy bands, respectively. A strong peak around 778.6 eV originated from the Co−S bonds implies the preparation of CoS.[26,27] Figure S3c displays the deconvolution of high-resolution XPS spectrum at S 2p region. The peaks at 161.6 and 162.5 eV were assigned to the S 2p3/2 and S 2p1/2 of CoS, respectively, and the binding energy at 163.9 eV was derived from the S_8 molecules confined within the nanostraws.[28] The smaller S 2p peaks at 167.5 and 168.8 eV confirm the presence of slightly oxidized sulfur species in S@CNTs/CoS-NSs.[29] According to the continuous weight loss from 200 to 350 °C by thermogravimetric analysis (TGA) under N_2 atmosphere (Figure S3d), the sulfur content in S@CNTs/CoS-NSs was determined to be 76.5 wt %.

For comparison, the control sample of CoS nanostraws without embedded CNTs was also prepared and denoted as CoS-NSs, as detailed in the Experimental Section. Moreover, commercial CNTs were also used as another control sample. As shown in Figure S4a, the CoS-NSs control sample displays the XRD peaks belonging to CoS, while the CNTs control sample only exhibits the wide and broad peak of carbon matrix. After filling sulfur into CoS-NSs and mixing sulfur with CNTs, the achieved control products were denoted as S@CoS-NSs and S/CNTs, respectively, and the preparation of these sulfur composites was confirmed by XRD analysis (Figure S4b). The morphology of CoS-NSs is similar to the CNTs/CoS-NSs, but the length is shorter (Figure S5a), and the CNTs control sample shows the typical nanotubular structure (Figure S5d). The S@CoS-NSs and S/CNTs (Figure S5b and e) well maintained the morphologies of initial samples, and the sulfur contents were measured to be 78.2 and 69.8 wt % (Figure S5c, f), respectively.

It is known that CoS possesses good electronic conductivity and high polarity that is beneficial to the adsorption of sulfur species.[30] To investigate the adsorption capability of CoS to sulfur species, theoretical simulations based on density function theory (DFT) method were conducted. Figure 2a displays the theoretical geometry configurations between the (101) planes of CoS and adsorbed sulfur species. The calculated binding energies of CoS with S_8, Li_2S, Li_2S_2, Li_2S_4, Li_2S_6, and Li_2S_8 are −1.99, −3.82, −3.24, −2.79, −3.11, and −3.54 eV, respectively, suggesting the strong chemisorption effect of CoS to sulfur species. Moreover, the adsorption capability of CNTs/CoS-NSs, CoS-NSs, and CNTs samples with polysulfides was experimentally evaluated by adding 10 mg of the sample into mixed dioxolane/dimethoxyethane (DOL/DME, 1:1 in volume) solution of 0.02 M Li_2S_4 (Figure 2b). The Li_2S_4 solutions mixed with CNTs/CoS-NSs and CoS-NSs turned from yellow to almost colorless within 30 min, while the Li_2S_4 solution mixed with CNTs only displays slight decoloration, confirming the high adsorption ability of CoS to sulfur species.

The capillary effect of CNTs/CoS-NSs to the Li−S electrolyte (Figure 2c−e) can be described by the Young−Laplace equation:

$$\rho g h \times \sin\theta = 2\gamma \times \cos\alpha / R \quad (1)$$

where ρ stands for the density of electrolyte, g represents the gravitational acceleration, h is the increased height of electrolyte level in CNTs/CoS-NSs induced by the capillary force, θ is the angle between CNTs/CoS-NSs and electrode surface, γ is the surface tension of electrolyte, α is the contact angle of electrolyte on CNTs/CoS-NSs surface, and R is the inner radius of CNTs/CoS-NSs. Eq 1 can be rewritten as

$$h = 2\gamma \times \cos\alpha / R\rho g \times \sin\theta \quad (2)$$

DOI: 10.1021/acsnano.8b01763
ACS Nano 2018, 12, 4868−4876

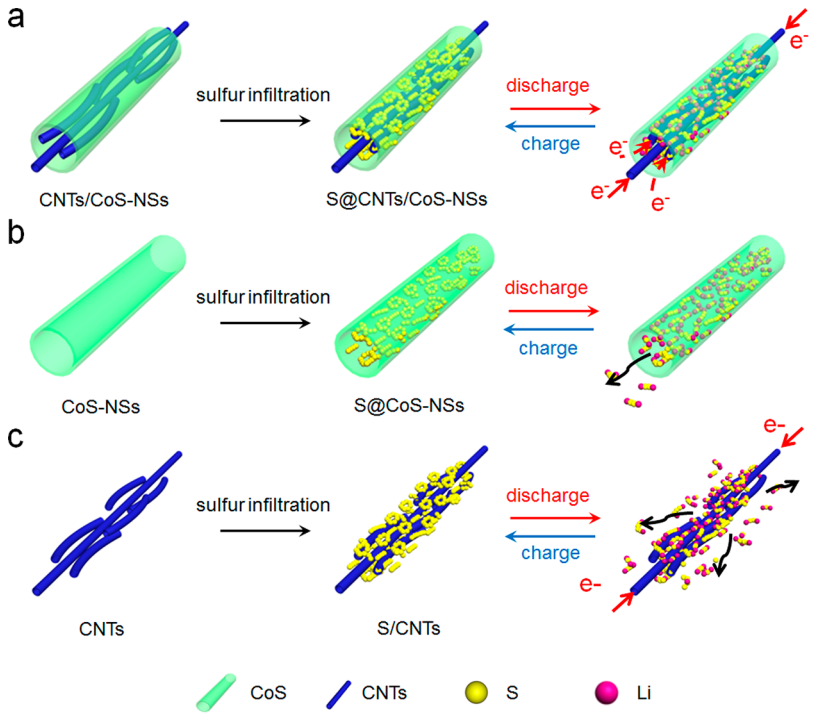

Figure 3. Comparison of the formation and reversible discharge−charge mechanisms of (a) S@CNTs/CoS-NSs, (b) S@CoS-NSs, and (c) S/CNTs cathodes, respectively.

In our case, $\gamma_{\text{Li-S electrolyte}}$ is 40.8×10^{-3} mN/m (provided by DodoChem. Regent Corp.), α is experimentally measured to be 25.3° (Figure 2d), ρ is $\sim 0.97 \times 10^3$ kg/m^3, g is 9.8 m/s^2, R is $\sim 100 \times 10^{-9}$ m, and θ is between 0 and 90°. Thus, the value of h can be calculated as

$$h = 77.6/\sin\theta \tag{3}$$

Assuming the nanostraw is placed vertically (θ = 90°), the minimum value of h can be estimated to be ~77.6 m, which is much higher than the actual length of CNTs/CoS-NSs, demonstrating the ultrastrong capillary effect that can well retain the Li−S electrolyte inside CNTs/CoS-NSs.

According to the above simulations, tests, and discussion, after the filling of sulfur and electrolyte into CNTs/CoS-NSs, the resultant S@CNTs/CoS-NSs cathode can take full advantage of closely combined CNTs and CoS components to restrict the shuttle effect of intermediate polysulfides through the physical confinement, chemisorption, and capillary effects (Figure 3a). In contrast, on condition that S@CoS-NSs and S/CNTs are used as sulfur cathodes, they could suffer from some apparent shortcomings compared to S@CNTs/CoS-NSs. Briefly, S@CoS-NSs cathode without CNTs may suffer from increased charge-transfer resistance and reduced sulfur utilization (Figure 3b),[31] while the S/CNTs cathode without CoS will result in severe polysulfide leakage and shuttle effect, due to the weak interactions between carbon matrix and sulfur species (Figure 3c).[32−34] These schematic diagrams demonstrate the high superiority of CNTs/CoS-NSs as a flexible sulfur host for Li−S batteries derived from the synergistic effect of these components.

The performances of S@CNTs/CoS-NSs and the control samples as sulfur cathodes in Li−S batteries were investigated by cyclic voltammetry (CV) and galvanostatic discharge−charge tests. Figure 4a presents the CV curves of S@CNTs/CoS-NSs cathode at a scan rate of 0.2 mV s^{-1}. Two cathodic peaks and one anodic peak were identified in the initial CV cycle. The reduction peak at 2.28 V was ascribed to the reduction of sulfur into high-order polysulfides (Li_2S_x, $4 \le x \le 8$), and the peak at 2.03 V was originated from the further reduction of high-order polysulfides into low-order polysulfides (Li_2S and Li_2S_2).[35,36] The single oxidation peak at 2.39 V indicates the one-step oxidation of Li_2S and/or Li_2S_2 into S_8.[37] In the following cycles, the S@CNTs/CoS-NSs cathode exhibits almost unchanged peak current densities, demonstrating the high reversibility. The CV curves of S@CoS-NSs and S/CNTs control samples measured under the same conditions are displayed in Figure S6a, c, respectively. In comparison, the S@CNTs/CoS-NSs cathode presents higher current density, indicating more efficient utilization of sulfur species (Figure S7a). The onset potential changes of all three redox peaks confirm the strong electrocatalytic effect of CNTs/CoS-NSs to the electrochemical redox conversion of sulfur species (Figure 5a−c). The onset potentials were taken at a current density of 10 μA cm^{-2} beyond the baseline current, following a classic definition in electrocatalysis (Figure 5d−f).[38] Compared to S@CoS-NSs and S/CNTs control samples, the adoption of S@CNTs/CoS-NSs increased the onset potentials of cathodic peaks, while decreased that of the anodic peak, indicating an accelerated electrocatalytic effect and improved polysulfide redox kinetics.[38]

The galvanostatic discharge−charge profiles of S@CNTs/CoS-NSs cathode under various current rates are shown in Figure 4b. The initial discharge curve exhibits the typical two plateaus associated with the formation of high-order polysulfides (Li_2S_x, $4 \le x \le 8$) at 2.32 V and low-order polysulfides (Li_2S and Li_2S_2) at 2.12 V, respectively, consistent with the CV results. As the current rate increases to 0.5, 1.0, 2.0, and 5.0 C, the galvanostatic discharge−charge profiles still remain similar features, suggesting the good performance under high rates. In contrast, the S@CoS-NSs and S/CNTs cathodes under high

DOI: 10.1021/acsnano.8b01763
ACS Nano 2018, 12, 4868−4876

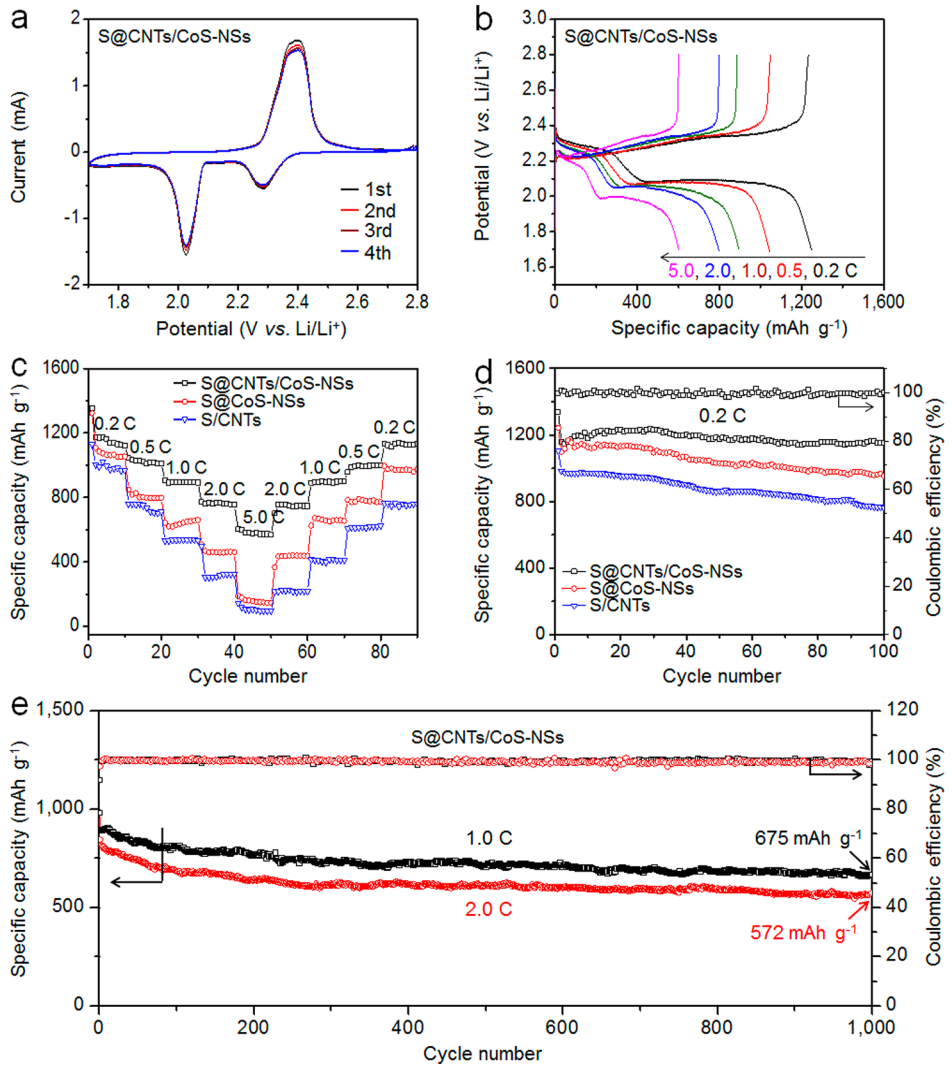

Figure 4. (a) CV curves of S@CNTs/CoS-NSs cathode at a scan rate of 0.2 mV s^{-1} within the voltage window of 1.7−2.8 V *vs* Li/Li^+. (b) Galvanostatic discharge−charge profiles of S@CNTs/CoS-NSs cathode at various current rates (0.2, 0.5, 1.0, 2.0, and 5.0 C). (c) Rate performances and (d) cycling performances of S@CNTs/CoS-NSs, S@CoS-NSs, and S/CNTs cathodes. (e) Long-term cycling stability and Coulombic efficiencies of S@CNTs/CoS-NSs cathodes at 1.0 and 2.0 C.

rates (Figure S6d, e) present much larger potential hysteresis, as compared in Figure S7b, further implying the superior electrocatalytic effect of CNTs/CoS-NSs for sulfur redox reactions.[38]

Figure 4c compares the rate performances of these cathodes. At 0.2 C, the S@CNTs/CoS-NSs cathode delivers an initial specific capacity of 1350 mAh g^{-1}, which is the highest among the samples (1321 mAh g^{-1} for S@CoS-NSs and 1130 mAh g^{-1} for S/CNTs). Moreover, except for S@CNTs/CoS-NSs, the specific capacities of other cathodes greatly decreased at high current rates. In detail, the specific capacities for S@CNTs/CoS-NSs cathode at 0.5, 1.0, 2.0, and 5.0 C are 1045, 907, 770, and 573 mAh g^{-1}, respectively, confirming the good rate capability, while the S@CoS-NSs and S/CNTs cathodes deliver much lower specific capacities of only 165 and 110 mAh g^{-1} at 5.0 C, respectively. The resistance characteristics of these cathodes were investigated by electrochemical impedance spectroscopy (EIS). The S@CNTs/CoS-NSs cathode exhibits very low charge-transfer resistance (Figure S8), which can facilitate the local and overall electron transportation and enhance the sulfur utilization.

The cycling performances of these cathodes at 0.2 C are shown in Figure 4d. The S@CNTs/CoS-NSs cathode exhibited the best cycling stability and retained highest discharge capacities. The specific capacity of S@CNTs/CoS-NSs was initially 1339 mAh g^{-1} and then kept at 1200 mAh g^{-1} after 40 cycles. After that, the specific capacity kept stable and finally maintained at 1154 mAh g^{-1} at the 100th cycle, corresponding to a capacity retention of about 86.2%. In contrast, the specific capacities of S@CoS-NSs and S/CNTs cathodes at the 100th cycle are 954 and 762 mAh g^{-1}, respectively, indicating lower cycling stability. To better illustrate the efficient utilization of sulfur in S@CNTs/CoS-NSs cathode, pristine CNTs/CoS-NSs cathode (without the filling of sulfur), as a control sample, was tested from 1.7 to 2.8 V *vs* Li/Li^+ (Figure S9). It verifies that the lithium storage capacity of pristine CNTs/CoS-NSs without sulfur is very low (only 20 mAh g^{-1} at 100 mA g^{-1}), thus has very little contribution to the total discharge capacity of Li−S batteries. Therefore, considering the achieved initial discharge capacity of 1339 mAh g^{-1} for S@CNTs/CoS-NSs cathode, the sulfur utilization ratio in S@CNTs/CoS-NSs cathode at the first cycle can be calculated to be ~80%. The

DOI: 10.1021/acsnano.8b01763
ACS Nano 2018, 12, 4868−4876

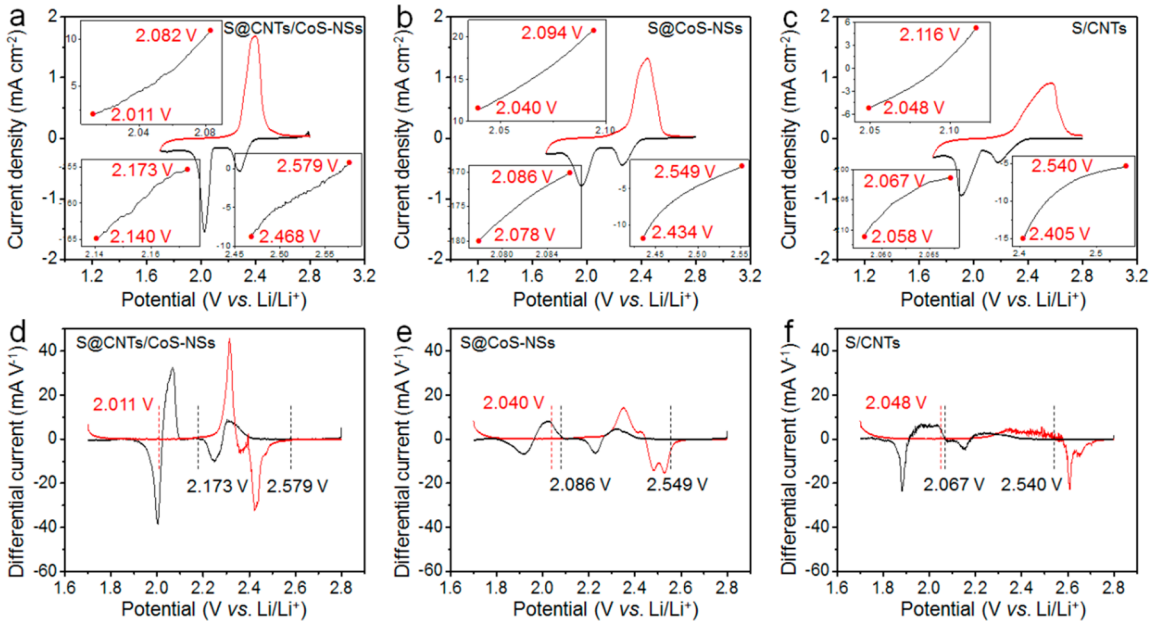

Figure 5. Electrocatalytic effects of CNTs/CoS-NSs host verified from the CV profiles. (a–c) CV curves and (d–f) differential CV curves of (a, d) S@CNTs/CoS-NSs, (b, e) S@CoS-NSs, and (c, f) S/CNTs cathodes. The corresponding onset potentials of redox peaks are provided in (a–c). The baseline potentials and baseline current densities in (d–f) are defined as the values before the redox peaks, where the variation on current density is the smallest, namely $dI/dV = 0$.

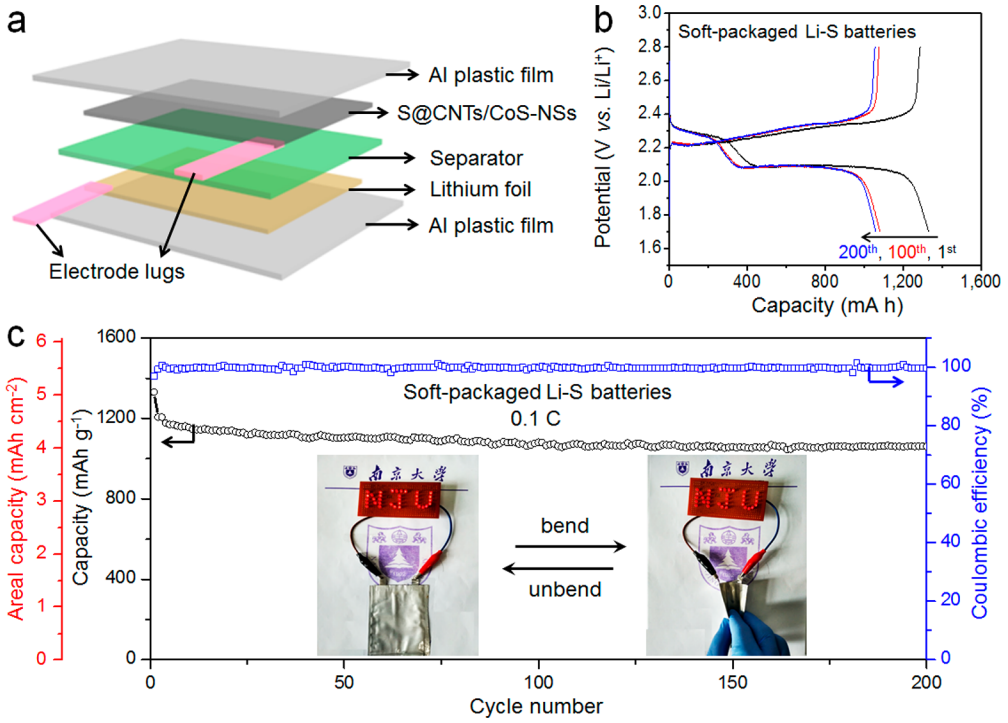

Figure 6. (a) Schematic diagrams of as-assembled soft-packed Li–S batteries. (b) Galvanostatic discharge–charge profiles of S@CNTs/CoS-NSs based soft-packed Li–S batteries at 0.1 C. (c) Cycling performance and Coulombic efficiencies of S@CNTs/CoS-NSs based soft-packed Li–S batteries at 0.1 C under continuous bending–unbending operations. The insets in (c) show the photographs of LED lamps with the pattern of "NJU" lighted by S@CNTs/CoS-NSs based soft-packed Li–S batteries upon bending–unbending operations. Logo used with permission.

resistance characteristics of these cathodes after cycling were investigated (Figure S10), and all the sulfur cathodes present the slightly increased charge-transfer resistances as compared with those before cycling. Moreover, the S@CNTs/CoS-NSs cathode exhibited the lowest charge-transfer resistance, further indicating the high electrical conductivity of CNTs/CoS-NSs.

The long-term cycling performance of Li–S batteries under high current rates is critical for practical applications. As shown in Figure 4e, the S@CNTs/CoS-NSs cathode at 1.0 C delivered an initial discharge capacity of 982 mAh g^{-1} and reached 708 mAh g^{-1} after 500 cycles. Finally, a high capacity of 675 mAh g^{-1} was achieved at the 1000th cycle,

DOI: 10.1021/acsnano.8b01763
ACS Nano 2018, 12, 4868–4876

corresponding to a capacity retention of 68.0% with the capacity decay of only 0.031% per cycle. As the current rate further increased to 2.0 C, the S@CNTs/CoS-NSs cathode still delivered good cycling stability with a high specific capacity of 572 mAh g^{-1} at the 1000th cycle, and the capacity decay retains at 0.032% per cycle. Moreover, the Coulombic efficiencies under 1.0 and 2.0 C were close to 100% even after 1000 cycles, indicating a very low amount of diffusion of polysulfides into the electrolyte.[38−40] To better demonstrate the suppression of shuttle effect by CNTs/CoS-NSs, the electrochemical performance of S@CNTs/CoS-NSs cathode at 1.0 and 2.0 C was investigated with no addition of $LiNO_3$ in the electrolyte. As presented in Figure S11, the Coulombic efficiencies of S@CNTs/CoS-NSs cathode at 1.0 and 2.0 C after 200 cycles are still nearly 100%, further indicating the successful suppression of polysulfide shuttle effect. The good cycling performance and high Coulombic efficiency stem from its structures and compositions of S@CNTs/CoS-NSs. Additionally, the structure integrity of S@CNTs/CoS-NSs cathode after long-term cycling was investigated. As illustrated in Figure S12, the S@CNTs/CoS-NSs cathode well maintained the initial structural features even after 1000 cycles, indicating its high structural integrity.

The S@CNTs/CoS-NSs with good flexibility and conductivity can serve as the sulfur cathode in flexible Li−S battery. As depicted in Figure 6a, the separator and electrolyte were sandwiched between the S@CNTs/CoS-NSs cathode and lithium foil and then sealed by Al plastic films. The performance stability of S@CNTs/CoS-NSs cathodes in soft-packed Li−S batteries was examined upon bending−unbending operations (Figure 6b, c and Video S1). The galvanostatic discharge−charge profiles under 0.1 C at the first, 100th, and 200th cycles are presented in Figure 6b, showing the typical two-plateau discharge characteristics. The corresponding Coulombic efficiencies were measured to be nearly 100% under bending−unbending (Figure 6c), suggesting that the polysulfide shuttle effect was well suppressed. The initial capacity reached 1330 mAh g^{-1}, and the areal capacity of soft-packed Li−S batteries was calculated to be 5.05 mAh cm^{-2}, which is higher than most of the reported flexible Li−S batteries.[20−25] The discharge capacity reached 1154 mAh g^{-1} (4.38 mAh cm^{-2}) at the 10th cycle, and thereafter kept almost stable after 200 cycles (1060 mAh g^{-1} and 4.03 mAh cm^{-2}) under continuous bending−unbending, suggesting the high flexibility and stable cyclability. To further demonstrate the practical potential *via* visual identification, the S@CNTs/CoS-NSs based soft-packed Li−S batteries were used to light a series of light-emitting diodes (LEDs) assembled to a pattern of "NJU" upon bending−unbending with almost no visual disparity, as displayed in the insets of Figure 6c and Video S1.

CONCLUSION

In summary, the crisscrossed network of hollow CNTs/CoS-NSs was prepared and proved to be an efficient sulfur host for flexible Li−S batteries. The key reasons to the high performance of S@CNTs/CoS-NSs cathode are (1) the interior hollow nanostructure provides a large inner void space to afford a high sulfur loading and accommodate the volume expansion of sulfur; (2) the high local and overall conductivity and the crisscrossed 3D conductive network can decrease the inner resistance and improve the sulfur utilization; (3) the high chemisorption and physical confinement to sulfur species can effectively suppress the shuttle effect; (4) the high lyophilicity and strong capillary effect induced by the nanostraws can well retain the Li−S electrolyte; and (5) the electrocatalytic effect of CoS facilitates the redox conversion of sulfur species. Benefiting from these merits, the S@CNTs/CoS-NSs cathodes exhibit impressive discharge capacity, rate capability, and cycling stability. Furthermore, the soft-packed Li−S batteries based on S@CNTs/CoS-NSs cathodes present great flexibility and high areal capacity. We expect the design concept of flexible Li−S batteries based on nanostraw-mat cathodes will provide favorable inspirations for integrating energy storage devices for smart wearable electronics.

EXPERIMENTAL SECTION

Preparation of Precursor CNTs/PAN Nanofibers. First, CNTs (TimeNano, Chengdu, China) were pretreated by refluxing in nitric acid solution (HNO_3, 1.0 M) at 80 °C for 3 h, washed several times in ethanol, and vacuum-dried under 60 °C. Briefly, 200 mg of polyacrylonitrile (PAN, M_s = 100,000, Sigma-Aldrich) was dissolved into 2.0 g of *N*,*N*-dimethylformamide (DMF) under vigorous stirring at 130 °C. After stirring for 30 min, 20 mg of CNTs powder was added into the above solution, and the resultant mixture was further stirred at room temperature for another 6 h. After that, precursor CNTs/PAN nanofibers were prepared by an electrospinning method, with the applied working voltage, flow rate, and distance between the syringe and collector fixed at 20 kV, 0.04 mm min^{-1}, and 18 cm, respectively.

Synthesis of CNTs/PAN/CoS Nanofibers. First, the precursor CNTs/PAN nanofibers were baked at 100 °C for several hours to improve the structural integrity. Then, 500 mg of cobalt acetate tetrahydrate ($Co(CH_3COO)_2{\cdot}4H_2O$) was dissolved into 80 mL of absolute ethanol. Subsequently, 50 mg of pretreated CNTs/PAN nanofibers was added into the above solution, and the achieved solution was stirred slowly at 80 °C for 6 h to allow the deposition of Co species onto the nanofibers. After that, the resultant product was washed with absolute ethanol for several times. For the synthesis of CNTs/PAN/CoS nanofibers, 100 mg of thioacetamide (TAA) and the above product were added into 35 mL of ethanol under stirring, then the mixture was transferred and sealed in a Teflon-lined autoclave and heated at 120 °C for 6 h. After cooling down to room temperature naturally, the precipitate was collected, washed with absolute ethanol for several times, and dried under vacuum at 60 °C overnight.

Preparation of CNTs/CoS-NSs. Briefly, 50 mg of CNTs/PAN/CoS nanofibers was added into 30 mL of aqueous solution containing 200 mg of glucose under stirring. Then the mixture was transferred into a Teflon-lined autoclave and heated at 200 °C for 8 h. After cooling down to room temperature naturally, the product was collected, washed with deionized water and ethanol for several times, and dried under vacuum at 60 °C overnight. Finally, the product was annealed at 500 °C for 2 h under N_2 atmosphere with a ramping rate of 1 °C min^{-1}.

Preparation of CoS-NSs Control Sample. The control sample of CoS-NSs (without CNTs) was prepared in the same way as CNTs/CoS-NSs but without the addition of CNTs.

Preparation of Sulfur Composites. Briefly, 30 mg of CNTs/CoS-NSs was added into CS_2 solution containing 150 mg of sulfur powder, and then the solution was stirred at room temperature for 4 h to remove the solvent. The as-obtained mixture was transferred into a Teflon-lined autoclave under Ar atmosphere and heated at 155 °C for 6 h. The as-obtained product was denoted as S@CNTs/CoS-NSs. As control samples, S@CoS-NSs and S/CNTs were also prepared in the same way as S@CNTs/CoS-NSs by using CoS-NSs and commercial CNTs as the starting materials, respectively.

Instruments and Characterizations. Scanning electron microscopy (SEM) images and energy dispersive X-ray spectroscopy (EDX) profiles were collected on a FEI Nova-450 instrument. Transmission electron microscopy (TEM), scanning TEM (STEM) images, and energy-filtered TEM (EFTEM) elemental mappings were taken on a JEOL JEM-2100F using an accelerating voltage of 200 kV. The contact angle was recorded with a DataPhysics OCA-30 instrument. The

DOI: 10.1021/acsnano.8b01763
ACS Nano 2018, 12, 4868−4876

powder X-ray diffraction (XRD) patterns were measured by an X-ray diffractometer (Bruker D-8 Advance) using Cu Kα (λ = 1.5406 Å) radiation at a scanning rate of 6° min^{-1}. X-ray photoelectron spectra (XPS) were performed on a PHI-5000 VersaProbe X-ray photoelectron spectrometer using an Al Kα X-ray radiation. Thermogravimetric analysis (TGA) was performed on a NETZSCH STA 449C instrument under N_2 atmosphere from room temperature to 600 °C at a heating rate of 10 °C min^{-1}.

Electrochemical Measurements. The working electrodes were prepared by mixing 80 wt % of sulfur composites, 10 wt % of acetylene black, and 10 wt % of polyvinylidene difluoride binder in *N*-methyl-2-pyrrolidone (NMP), and the slurry was coated on an aluminum foil and vacuum dried at 60 °C overnight. The Li−S coin cells were assembled in an argon-filled glovebox with the above-prepared sulfur cathodes and lithium foil anodes. In the coin cells, the areal sulfur loading of cathodes is 1.0−1.5 mg cm^{-2}. A solution of 1.0 M bis(trifluoro-methane)sulfonamide lithium (LiTFSI) dissolved in a mixed solvent of 1,2-dimethoxyethane (DME) and 1,3-dioxolane (DOL) (1:1 in volume, with 1.0 wt % $LiNO_3$ additive) was used as the electrolyte. For the assembly of pouch-type soft-packed Li−S batteries (sulfur loading mass of 3.8 mg cm^{-2}), the separator and the electrolyte were sandwiched by the S@CNTs/CoS-NSs cathode and lithium foil and then sealed by Al plastic films.

The cyclic voltammograms (CV) curves were collected on a Chenhua CHI-760E electrochemical workstation at a scan rate of 0.2 mV s^{-1} between 1.8 and 2.7 V. The cycling performance of Li−S batteries was measured on a LAND CT2001A analyzer at different current rates with a potential window of 1.7−2.8 V *vs* Li/Li$^+$. The EIS analysis was carried out in the range from 100 kHz to 0.01 Hz.

Computational Methods. Density functional theory (DFT) method was employed to calculate the binding energies (E_b) between the sulfur host material and the polysulfides, which is defined by

$$E_{ads} = E_{s+host} - E_s - E_{host} \quad (4)$$

where E_{s+host}, E_s, and E_{host} are the energies of the polysulfides-host material, polysulfides, and host material, respectively. The initial conformation of all molecules was obtained by molecular mechanics (MM) method (Forcite module). The DFT calculations were performed in the Dmol3 module of Accelrys Material Studio. The exchange−correlation functional was approximated by the Perdew−Burke−Ernzerhof method. The DFT semicore pseudopotentials were used to calculate the core−electron interactions. The DFT-D (D stands for dispersion) approach with the Ortmann−Bechstedt−Schmidt vdW correction was used to accurately describe the vdW interactions, which influence the adsorption geometry configurations of Li_2S_x species on host material. The solvation effect was considered by the COSMO model with a dielectric constant of 6.18 to mimic the mixed DME/DOL solvent.

ASSOCIATED CONTENT

Supporting Information

The Supporting Information is available free of charge on the ACS Publications website at DOI: 10.1021/acsnano.8b01763.

Figures S1−S12 (PDF)

Video S1 (AVI)

AUTHOR INFORMATION

Corresponding Author

*E-mail: zhongjin@nju.edu.cn.

ORCID

Tao Chen: 0000-0003-2536-4145

Jie Liu: 0000-0003-0451-6111

Zhong Jin: 0000-0001-8860-8579

Notes

The authors declare no competing financial interest.

ACKNOWLEDGMENTS

This work is supported by National Key R&D Program of China (2017YFA0208200, 2016YFB0700600), Projects of NSFC (21573108, 51761135104), Natural Science Foundation of Jiangsu Province (BK20150583, BK20170644), High-Level Entrepreneurial and Innovative Talents Program of Jiangsu Province, and the Fundamental Research Funds for the Central Universities (020514380107).

REFERENCES

(1) Cheng, F.; Liang, J.; Tao, Z.; Chen, J. Functional Materials for Rechargeable Batteries. *Adv. Mater.* **2011**, *23*, 1695−1715.

(2) Kaskhedikar, N. A.; Maier, J. Lithium Storage in Carbon Nanostructures. *Adv. Mater.* **2009**, *21*, 2664−2680.

(3) Tarascon, J.-M.; Recham, N.; Armand, M.; Chotard, J. N.; Barpanda, P.; Walker, W.; Dupont, L. Hunting for Better Li-Based Electrode Materials *via* Low Temperature Inorganic Synthesis. *Chem. Mater.* **2010**, *22*, 724−739.

(4) Manthiram, A.; Chemelewski, K.; Lee, E. S. A Perspective on the High-Voltage $LiMn_{1.5}Ni_{0.5}O_4$ Spinel Cathode for Lithium-Ion Batteries. *Energy Environ. Sci.* **2014**, *7*, 1339−1350.

(5) Tang, Y.; Zhang, Y.; Li, W.; Ma, B.; Chen, X. Rational Material Design for Ultrafast Rechargeable Lithium-Ion Batteries. *Chem. Soc. Rev.* **2015**, *44*, 5926−5940.

(6) Song, M. K.; Zhang, Y. G.; Cairns, E. J. A Long-Life, high-Rate Lithium/Sulfur Cell: A Multifaceted Approach to Enhancing Cell Performance. *Nano Lett.* **2013**, *13*, 5891−5899.

(7) Scrosati, B.; Hassoun, J.; Sun, Y. K. Lithium-Ion Batteries. A Look Into the Future. *Energy Environ. Sci.* **2011**, *4*, 3287−3295.

(8) Bruce, P. G.; Freunberger, S. A.; Hardwick, L. J.; Tarascon, J. M. Li-O_2 and Li-S Batteries with High Energy Storage. *Nat. Mater.* **2012**, *11*, 19−29.

(9) Manthiram, A.; Fu, Y.; Su, Y. S. Challenges and Prospects of Lithium-Sulfur Batteries. *Acc. Chem. Res.* **2013**, *46*, 1125−1134.

(10) Yang, Y.; Zheng, G.; Cui, Y. Nanostructured Sulfur Cathodes. *Chem. Soc. Rev.* **2013**, *42*, 3018−3032.

(11) Peng, H. J.; Zhang, Z. W.; Huang, J. Q.; Zhang, G.; Xie, J.; Xu, W. T.; Shi, J. L.; Chen, X.; Cheng, X. B.; Zhang, Q. A Cooperative Interface for Highly Efficient Lithium-Sulfur Batteries. *Adv. Mater.* **2016**, *28*, 9551−9558.

(12) Manthiram, A.; Fu, Y.; Chung, S. H.; Zu, C.; Su, Y.-S. Rechargeable Lithium−Sulfur Batteries. *Chem. Rev.* **2014**, *114*, 11751−11787.

(13) Cao, Q.; Rogers, J. A. Ultrathin Films of Single-Walled Carbon Nanotubes for Electronics and Sensors: A Review of Fundamental and Applied Aspects. *Adv. Mater.* **2009**, *21*, 29−53.

(14) Bae, S.; Kim, H.; Lee, Y.; Xu, X. F.; Park, J. S.; Zheng, Y.; Balakrishnan, J.; Lei, T.; Kim, H. R.; Song, Y. I.; Kim, Y. J.; Kim, K. S.; Ozyilmaz, B.; Ahn, J. H.; Hong, B. H.; Iijima, S. Roll-to-Roll Production of 30-Inch Graphene Films for Transparent Electrodes. *Nat. Nanotechnol.* **2010**, *5*, 574−578.

(15) Kim, D. H.; Viventi, J.; Amsden, J. J.; Xiao, J. L.; Vigeland, L.; Kim, Y. S.; Blanco, J. A.; Panilaitis, B.; Frechette, E. S.; Contreras, D.; Kaplan, D. L.; Omenetto, F. G.; Huang, Y. G.; Hwang, K. C.; Zakin, M. R.; Litt, B.; Rogers, J. A. Dissolvable Films of Silk Fibroin for Ultrathin, Conformal Bio-Integrated Electronics. *Nat. Mater.* **2010**, *9*, 511−517.

(16) Kim, D. H.; Lu, N. S.; Ma, R.; Kim, Y. S.; Kim, R. H.; Wang, S. D.; Wu, J.; Won, S. M.; Tao, H.; Islam, A.; Yu, K. J.; Kim, T. I.; Chowdhury, R.; Ying, M.; Xu, L. Z.; Li, M.; Chung, H. J.; Keum, H.; McCormick, M.; Liu, P.; Zhang, Y. W.; Omenetto, F. G.; Huang, Y. G.; Coleman, T.; Rogers, J. A. Epidermal Electronics. *Science* **2011**, *333*, 838−843.

(17) Kaltenbrunner, M.; Sekitani, T.; Reeder, J.; Yokota, T.; Kuribara, K.; Tokuhara, T.; Drack, M.; Schwodiauer, R.; Graz, I.; Bauer-Gogonea, S.; Bauer, S.; Someya, T. Bauer S.; Someya, T. An Ultra-Lightweight Design for Imperceptible Plastic Electronics. *Nature* **2013**, *499*, 458−463.

DOI: 10.1021/acsnano.8b01763
ACS Nano 2018, 12, 4868−4876

(18) Tee, B. C. K.; Chortos, A.; Berndt, A.; Nguyen, A. K.; Tom, A.; McGuire, A.; Lin, Z. L. C.; Tien, K.; Bae, W. G.; Wang, H. L.; Mei, P.; Chou, H. H.; Cui, B. X.; Deisseroth, K.; Ng, T. N.; Bao, Z. N. A Skin-Inspired Organic Digital Mechanoreceptor. *Science* **2015**, *350*, 313−316.
(19) Peng, H. J.; Huang, J. Q.; Zhang, Q. A Review of Flexible Lithium-Sulfur and Analogous Alkali Metal-Chalcogen Rechargeable Batteries. *Chem. Soc. Rev.* **2017**, *46*, 5237−5288.
(20) Mao, Y. Y.; Li, G. R.; Guo, Y.; Li, Z. P.; Liang, C. D.; Peng, X. S.; Lin, Z. Foldable Interpenetrated Metal-Organic Frameworks/Carbon Nanotubes Thin Film for Lithium-Sulfur Batteries. *Nat. Commun.* **2017**, *8*, 14628.
(21) Cao, J.; Chen, C.; Zhao, Q.; Zhang, N.; Lu, Q. Q.; Wang, X. Y.; Niu, Z. Q.; Chen, J. A Flexible Nanostructured Paper of a Reduced Graphene Oxide-Sulfur Composite for High-Performance Lithium-Sulfur Batteries with Unconventional Configurations. *Adv. Mater.* **2016**, *28*, 9629−9636.
(22) Yu, M. L.; Wang, Z. Y.; Wang, Y. W.; Dong, Y. F.; Qiu, J. S. Freestanding Flexible Li_2S Paper Electrode with High Mass and Capacity Loading for High-Energy Li−S Batteries. *Adv. Energy Mater.* **2017**, *7*, 1700018.
(23) Xiao, P. T.; Bu, F. X.; Yang, G. H.; Zhang, Y.; Xu, Y. X. Integration of Graphene, Nano Sulfur, and Conducting Polymer into Compact, Flexible Lithium-Sulfur Battery Cathodes with Ultrahigh Volumetric Capacity and Superior Cycling Stability for Foldable Devices. *Adv. Mater.* **2017**, *29*, 1703324.
(24) Xiang, M. W.; Wu, H.; Liu, H.; Huang, J.; Zheng, Y. F.; Yang, L.; Jing, P.; Zhang, Y.; Dou, S. X.; Liu, H. K. A Flexible 3D Multifunctional MgO-Decorated Carbon Foam@CNTs Hybrid as Self-Supported Cathode for High-Performance Lithium-Sulfur Batteries. *Adv. Funct. Mater.* **2017**, *27*, 1702573.
(25) Liu, R. Q.; Liu, Y. J.; Chen, J.; Kang, Q.; Wang, L. L.; Zhou, W. X.; Huang, Z. D.; Lin, X. J.; Li, Y.; Li, P.; Feng, X. M.; Wu, G.; Ma, Y. W.; Huang, W. Flexible Wire-Shaped Lithium-Sulfur Batteries with Fibrous Cathodes Assembled *via* Capillary Action. *Nano Energy* **2017**, *33*, 325−333.
(26) Alstrup, I.; Chorkendorff, I.; Candia, R.; Clausen, B. S.; TopsØe, H. A Combined X-Ray Photoelectron and Mössbauer Emission Spectroscopy Study of the State of Cobalt in Sulfided, Supported, and Unsupported Co-Mo Catalysts. *J. Catal.* **1982**, *77*, 397−409.
(27) Kośanyi, T. I.; Manninger, I.; Páal, Z.; Marks, O.; Gunter, J. R. Activation of Unsupported Co-Mo Catalysts in Thiophene Hydrodesulfurization. *J. Catal.* **1989**, *116*, 422−439.
(28) Rehman, S.; Gu, X. X.; Khan, K.; Mahmood, N.; Yang, W. L.; Huang, X. X.; Guo, S. J.; Hou, Y. L. 3D Vertically Aligned and Interconnected Porous Carbon Nanosheets as Sulfur Immobilizers for High Performance Lithium-Sulfur Batteries. *Adv. Energy Mater.* **2016**, *6*, 1502518.
(29) Pang, Q.; Tang, J. T.; Huang, H.; Liang, X.; Hart, C.; Tam, K. C.; Nazar, L. F. A Nitrogen and Sulfur Dual-Doped Carbon Derived from Polyrhodanine@Cellulose for Advanced Lithium-Sulfur Batteries. *Adv. Mater.* **2015**, *27*, 6021−6028.
(30) Lai, C. H.; Lu, M. Y.; Chen, L. J. Metal Sulfide Nanostructures: Synthesis, Properties and Applications in Energy Conversion and Storage. *J. Mater. Chem.* **2012**, *22*, 19−30.
(31) Liu, Y. Z.; Li, G. R.; Fu, J.; Chen, Z. W.; Peng, X. S. Strings of Porous Carbon Polyhedrons as Self-Standing Cathode Host for High-Energy-Density Lithium-Sulfur Batteries. *Angew. Chem., Int. Ed.* **2017**, *56*, 6176−6180.
(32) Zu, C.; Fu, Y.; Manthiram, A. Highly Reversible Li/Dissolved Polysulfide Batteries with Binder-Free Carbon Nanofiber Electrodes. *J. Mater. Chem. A* **2013**, *1*, 10362−10367.
(33) Guo, J.; Xu, Y.; Wang, C. Sulfur-Impregnated Disordered Carbon Nanotubes Cathode for Lithium-Sulfur Batteries. *Nano Lett.* **2011**, *11*, 4288−4294.
(34) Ji, L.; Rao, M.; Aloni, S.; Wang, L.; Cairns, E. J.; Zhang, Y. Porous Carbon Nanofiber-Sulfur Composite Electrodes for Lithium/Sulfur Cells. *Energy Environ. Sci.* **2011**, *4*, 5053−5059.
(35) Liang, X.; Zhang, M.; Kaiser, M. R.; Gao, X.; Konstantinov, K.; Tandiono, R.; Wang, Z.; Liu, H. K.; Dou, S. X.; Wang, J. Split-Half-Tubular Polypyrrole@Sulfur@Polypyrrole Composite with A Novel Three-Layer-3D Structure as Cathode for Lithium/Sulfur Batteries. *Nano Energy* **2015**, *11*, 587−599.
(36) Zhou, G.; Zhao, Y.; Manthiram, A. Dual-Confined Flexible Sulfur Cathodes Encapsulated in Nitrogen-Doped Double-Shelled Hollow Carbon Spheres and Wrapped with Graphene for Li-S batteries. *Adv. Energy Mater.* **2015**, *5*, 1402263.
(37) Zhou, W.; Wang, C.; Zhang, Q.; Abruna, H. D.; He, Y.; Wang, J.; Mao, S. X.; Xiao, X. Tailoring Pore Size of Nitrogen-Doped Hollow Carbon Nanospheres for Confining Sulfur in Lithium-Sulfur batteries. *Adv. Energy Mater.* **2015**, *5*, 1401752.
(38) Ma, L. B.; Yuan, H.; Zhang, W. J.; Zhu, G. Y.; Wang, Y. R.; Hu, Y.; Zhao, P. Y.; Chen, R. P.; Chen, T.; Liu, J.; Hu, Z.; Jin, Z. Porous-Shell Vanadium Nitride Nanobubbles with Ultrahigh Areal Sulfur Loading for High-Capacity and Long-Life Lithium-Sulfur Batteries. *Nano Lett.* **2017**, *17*, 7839−7846.
(39) Ma, L. B.; Chen, R. P.; Zhu, G. Y.; Hu, Y.; Wang, Y. R.; Chen, T.; Liu, J.; Jin, Z. Cerium Oxide Nanocrystal Embedded Bimodal Micromesoporous Nitrogen-Rich Carbon Nanospheres as Effective Sulfur Host for Lithium-Sulfur Batteries. *ACS Nano* **2017**, *11*, 7274−7283.
(40) Liang, X.; Nazar, L. F. *In Situ* Reactive Assembly of Scalable Core-Shell Sulfur-MnO_2 Composite Cathodes. *ACS Nano* **2016**, *10*, 4192−4198.

DOI: 10.1021/acsnano.8b01763
ACS Nano 2018, 12, 4868−4876